

RESEARCH ARTICLE

The emergence of a complex pore-canal system in the dermal skeleton of *Tremataspis* (Osteostraci)

Oskar Bremer¹  | Qingming Qu^{2,3} | Sophie Sanchez^{1,4} | Tiiu Märss⁵ | Vincent Fernandez⁶  | Henning Blom¹

¹Department of Organismal Biology, Uppsala University, Uppsala, Sweden

²Department of Biology, University of Ottawa, Ottawa, Ontario, Canada

³State Key Laboratory of Cellular Stress Biology, Innovation Center for Cell Signal Network, School of Life Sciences, Xiamen University, Xiamen, China

⁴European Synchrotron Radiation Facility, Grenoble, France

⁵Department of Geology, Tallinn University of Technology, Tallinn, Estonia

⁶Imaging and Analysis Centre, Natural History Museum, London, UK

Correspondence

Oskar Bremer, Department of Organismal Biology, Uppsala University, Uppsala, Sweden.
Email: bremer.oskar@gmail.com

Abstract

Thyestiids are a group of osteostracans (sister-group to jawed vertebrates) ranging in time from the early Silurian to Middle Devonian. *Tremataspis* is unique among thyestiids in having a continuous mesodentine and enameloid cover on its dermal elements, and an embedded pore-canal system divided into lower and upper parts by a perforated septum. The origin of this upper mesh canal system and its potential homology to similar canal systems of other osteostracans has remained a matter of debate. To investigate this, we use synchrotron radiation microtomography data of four species of *Tremataspis* and three other thyestiid genera. *Procephalaspis oeselensis* lacks an upper mesh canal system entirely, but *Aestiaspis viitaensis* has partially enclosed upper canals formed between slightly modified tubercles that generally only cover separate pore fields. Further modification of tubercles in *Dartmuthia gemmifera* forms a more extensive, semi-enclosed upper mesh canal system that overlies an extensive perforated septum, similar to that found in *Tremataspis*. Lower mesh canals in *P. oeselensis* are radially arranged and buried tubercles indicate a continuous growth and addition of dermal hard tissues. These features are lacking to varying degrees in the other investigated thyestiids, and *Tremataspis* probably had a determinate growth accompanied by a single mineralization phase of its dermal hard tissues. The previously proposed homology between the semi-enclosed upper canal system in *Dartmuthia* to the pore-canal system in *Tremataspis* is supported in this study, but the suggested homologies between these canals and other parts of the thyestiid vasculature to those in non-thyestiid osteostracans remain unclear. This study shows that three-dimensional modeling of high-resolution data can provide histological and structural details that can help clarify homology issues and elucidate the evolution of dermal hard tissues in osteostracans. In extension, this can give insights into how these tissues relate to those found among jawed vertebrates.

KEYWORDS

3D histology, dermal hard tissues, Thyestiida

This is an open access article under the terms of the Creative Commons Attribution License, which permits use, distribution and reproduction in any medium, provided the original work is properly cited.

© 2021 The Authors. *Journal of Morphology* published by Wiley Periodicals LLC.

1 | INTRODUCTION

Osteostracans are an extinct group of jawless vertebrates generally considered the sister-group to jawed vertebrates (Sansom, 2009). As such, they bridge the phylogenetic gap between living jawless and jawed vertebrates (gnathostomes). Like many stem-gnathostomes, but unlike living jawless vertebrates, osteostracans had a dermal skeleton composed of three layers: a superficial layer formed by an odontogenic component, as well as middle and basal layers formed by an osteogenic component (O'Shea et al., 2019; Smith & Hall, 1993). It is therefore important to understand the organization and development of osteostracan dermal hard-tissues in order to elucidate the early evolution of vertebrate hard tissues and the dermal skeleton.

The superficial layer in osteostracans is composed of a type of dentine called mesodentine (Ørvig, 1967), which is supplied by the subepidermal vascular plexus (Stensiö, 1932), and sometimes has a hypermineralized cap called enameloid (Denison, 1947; Stensiö, 1927). The vascularized middle layer has generally been identified as cellular bone with concentrically arranged osteocytes and lamellae around canals (Denison, 1947; Gross, 1935, 1956; O'Shea et al., 2019; Qu et al., 2015; Stensiö, 1927). The basal layer is composed of a plywood-like lamellar tissue that has been suggested to be cellular bone (Denison, 1947; Gross, 1935, 1956; Ørvig, 1967; Stensiö, 1927), isopedin (Donoghue et al., 2006; Gross, 1956, 1968a, 1968b), elasmodine or ossification of the stratum compactum (Sire et al., 2009). Wang et al. (2005) recognized it as acellular, with the putative cell-spaces being mere gaps formed between the fiber bundles, which was corroborated by O'Shea et al. (2019). For a thorough review of previous histological studies of *Tremataspis*, and osteostracans in general, the reader is referred to O'Shea et al. (2019).

Thyestiida Berg (1940) is a derived group of osteostracans known from the lower Silurian of Europe to Middle Devonian of Central Asia (Sansom, 2008). Among the thyestiids, *Tremataspis* has often intrigued researchers because of the extensive pore-canal system in its dermal skeleton (Denison, 1947, 1951; Gross, 1935; Stensiö, 1927; Wängsjö, 1946). This system has a polygonal architecture and is divided into lower and upper parts by a perforated septum (Börlau, 1951; Denison, 1947). Previous histological studies have identified the semi-enclosed upper canal system of the thyestiid *Dartmuthia gemmifera* as closely related to the pore-canal system of *Tremataspis* (e.g., Afanassieva, 1995; Denison, 1951). In *D. gemmifera*, these partially enclosed canals formed at junctions between tesserae, although many of these appear not to be proper tesserae but modified and plate-like tubercles (see Gross, 1961; Wängsjö, 1946). Some studies have also homologized the pore-canal system of *Tremataspis* to the inter- and intra-areal canals that are found between and within tesserae, respectively, in cephalaspid osteostracans (Denison, 1951; Stensiö, 1927, 1932). In fact, the presence of polygonal canals in many osteostracans, ranging from fully enclosed canals to open grooves, led Stensiö (1932) to suggest that such a network existed in soft tissues and drove the division of hard tissue vasculature into polygonal areas. However, the correlation between the architecture of these superficial canals to the underlying dermal skeleton was not always evident according to Wängsjö (1952). The pore-canal system in *Tremataspis* is not only superficially similar to the convergently acquired, hard tissue-embedded pore-

canal system of cephalaspid osteostracans (e.g., Stensiö, 1927), but also to the cosmine of extinct osteichthyans (e.g., Mondéjar-Fernández, 2018; Qu et al., 2017; Schultze, 2016). Similarly, the true functional role of the pore-canal system in *Tremataspis* has remained unclear, with suggestions ranging from mucous canals (Stensiö, 1932) or extensions of the lateral lines (Börlau, 1951; Denison, 1947, 1966) to a system for electroreceptors (Thomson, 1977). King et al. (2018) reviewed and discussed these previous suggestions and refuted an electroreceptive role for the pore-canal system, leaning more toward a mechanoreceptive function similar to lateral lines. This view, however, was not shared by O'Shea et al. (2019), who thoroughly investigated the three-dimensional (3D) histology of a single specimen of *Tremataspis mammillata* and discussed its potential development and function.

In this study, we use propagation phase contrast synchrotron X-ray micro computed tomography (PPC-SR μ CT) to analyze the 3D histology of the dermal skeleton of four different species of *Tremataspis* and the closely related *D. gemmifera*, as well as the other thyestiids *Procephalaspis oeselensis* and *Aestiaspis viitaensis*. Interpreting this in the phylogenetic context established for thyestiids (Sansom, 2008, 2009) enables us to infer the emergence of the complex pore-canal system in *Tremataspis* through the modification of the structures already present in other taxa.

2 | MATERIALS AND METHODS

The material for this study comes from the mid-Silurian of Saaremaa Island, Estonia, from the collection sampled by Tiiu Märss between 1970 and 2010. The *P. oeselensis* head shield fragment (GIT 769-17) comes from Silma pank locality, the *A. viitaensis* shield fragment (GIT 769-29) comes from Elda cliff (Bed 5), the *D. gemmifera* head shield fragment (GIT 769-25) and scale (GIT 769-24), as well as the *T. mammillata* (GIT 769-20) head shield fragment come from the Himmiste Quarry, the *Tremataspis milleri* (GIT 769-1) shield fragment comes from Vesiku creek, and the *Tremataspis schmidtii* (GIT 769-11) shield fragment and the *Tremataspis perforata* scales (GIT 769-15 and 769-16) come from the Viita trench locality. The rock samples were subjected to acetic acid preparation and numerous microfossils were sorted from the residues. The head shield fragments and scales were identified following the taxonomic framework established by Märss et al. (2014). The specimens are housed at the Department of Geology, Tallinn University of Technology, Estonia.

All specimens were imaged using PPC-SR μ CT at the ID19 beamline of the European Synchrotron Radiation Facility (Grenoble, France). The experimental setup consisted of: filtered white beam from a wiggler (W150B gap = 60 mm; filters: Al 2.8 mm, W 0.14 mm) which generated a spectrum with a total integrated detected energy of 69 keV; an indirect detector comprising a LuAG 0.25 μ m scintillator, mirror reflecting the image upward, a $\times 10$ Mitutoyo lens (Mitutoyo corporation, Kawasaki, Japan) and a PCO. edge 4.2 (PCO, Kelheim, Germany) scientific Complementary metal-oxide-semiconductor (sCMOS) detector with USB3 camera link. Tomographic acquisitions consisted of 2999 projections over a 360° rotation of the sample and an exposure time of 0.1 s per projection. In some cases, to increase the horizontal field of view (hFOV), the center of rotation was shifted by

0.65 mm, effectively doubling the hFOV. The sample detector distance was set to 100 mm, resulting in a measured isotropic pixel size on radiograph of 0.716 ± 0.01 mm. Additionally, two white field images (with no sample in the field of view), representing the intensity of the beam at the beginning and end of the acquisition, were generated from the median of 41 projections; a dark field image (no incoming X-ray, measuring only the noise of the camera) was generated from the average of 40 projections. Computed tomographic reconstruction was performed using the single distance phase retrieval approach (Paganin et al., 2002) of PyHST2 (Mirone et al., 2014). Parameters for phase retrieval were intentionally set with low values ($\delta/\beta = 50$), effectively using the approach as a denoising low-pass filter. From the 32-bit data generated by PyHST2, post-processing included: data conversion as 16-bit jpeg2000 stack with a compression ratio of 10, using the full 3D histogram and excluding 0.001% on both extremities; ring correction (Lyckegaard et al., 2011).

The reconstructed data were imported as jpeg2000 stacks into the software VGStudio Max 3.4 (Volume Graphics GmbH) installed on a Dell Computer Station Precision T7600 running Windows 7. The 3D-models presented in this work were created from regions of interest using selection tools in VGStudio Max 3.4. Virtual scan slices and images of the 3D-models were rendered in VGStudio Max 3.4 and exported using the export tool. These were then assembled in Adobe Photoshop CC 2015 and Adobe Illustrator CC 2015 (Adobe Inc. San Jose, CA) to create the figures.

3 | RESULTS

The general structure of the dermal skeleton is clearly visible in virtual scan slices of the elements (Figure 1), and its three layers are labeled in Figure 1(c). The basal layer consists of laminae composed of fiber bundles with rounded to rectangular cross-sections that are almost orthogonally orientated compared to underlying and overlying laminae (Figure 1(c),(d)).

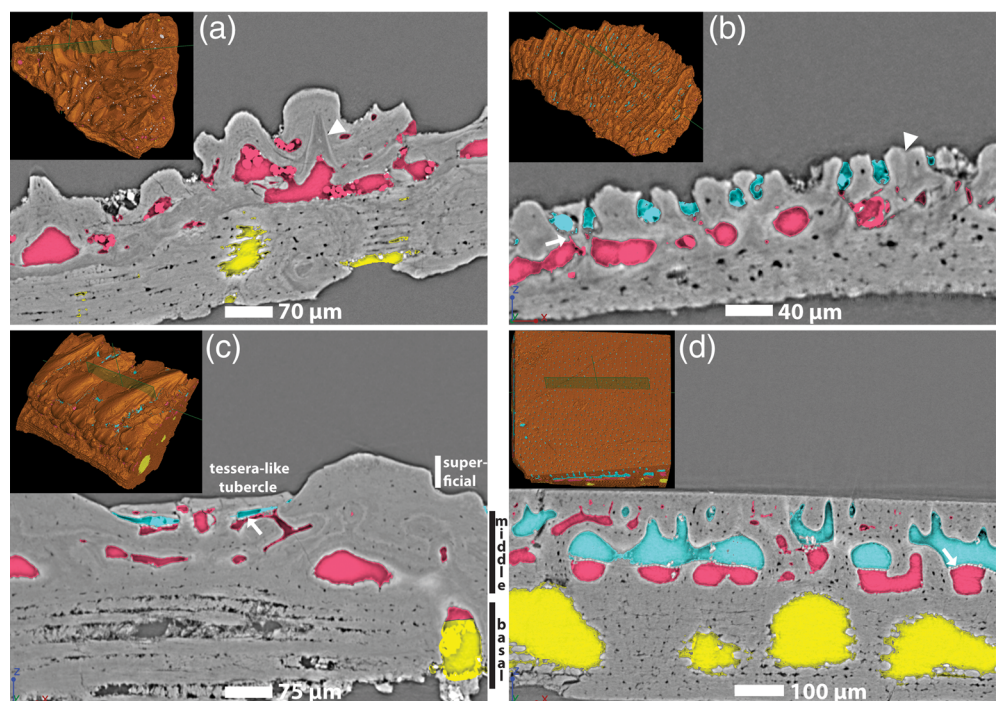
The basal layer is usually distinct because of its difference in architecture, but the boundary to the middle layer can sometimes be uneven (Figure 1(a)). The middle layer varies in thickness between taxa and has dispersed cell spaces and lines around its canals (e.g., Figure 1(c)), that have often been identified as osteon-like structures. The transition between the middle and superficial layers is often hard to distinguish given the similar structure of mesodentine and cellular bone. However, the more dentine-like tissue, and especially the hypermineralized cap, is generally only present in the apex of large tubercles (e.g., Figure 1(c)), but covers the whole surface in *Tremataspis* (Figure 1(d)).

The terminology in this study for the canal systems within the three layers described above will follow the one adapted by Qu et al. (2015) from earlier works. These are basal cavities and canals in the laminated basal layer (Figure 1: yellow), mesh canals (Figure 1: pink) in the middle layer (divided into lower and upper [Figure 1: teal] parts in *Tremataspis*), and the subepidermal vascular plexus (also colored pink in the figures) that arise from the mesh canals and supply the dentine of the superficial layer. Note that the partially enclosed canals above the pore fields in *A. viitaensis* and *D. gemmifera* (called partially or semi-enclosed upper canals in this study) are also highlighted in teal (Figure 1(b),(c)). The differently sized polygons of upper mesh canals in the *Tremataspis* taxa have historically been referred to as inter- and intra-areal canals after being homologized with the canals found in cephalaspids (Denison, 1951; Stensiö, 1927, 1932). However, they will here be referred to as polygonal and intra-polygonal canals to avoid assumptions of homology.

3.1 | *Procephalaspis oeselensis*

One of the most striking features of the head shield fragment of *P. oeselensis* are the buried surfaces (Figure 1(a), arrowhead). Three-dimensional models of the fragment (Figure 2) show that these buried

FIGURE 1 Virtual scan slices and inserts of their respective positions on the dermal elements. The different canal systems are highlighted in yellow (basal cavities and canals), pink (lower mesh canals), and teal (upper canals/upper mesh canals). (a), *Procephalaspis oeselensis* head shield fragment (GIT 769-17); (b), *Aestiaspis viitaensis* head shield fragment (GIT 769-29); (c), *Dartmouthia gemmifera* scale (GIT 769-24); (d), *Tremataspis milleri* head shield fragment (GIT 769-1). The basal, middle, and superficial layers are indicated in (c). Arrowheads in (a) and (b) indicate overgrowth of tubercles, and arrows in (b)–(d) point to the pore field and perforated septum



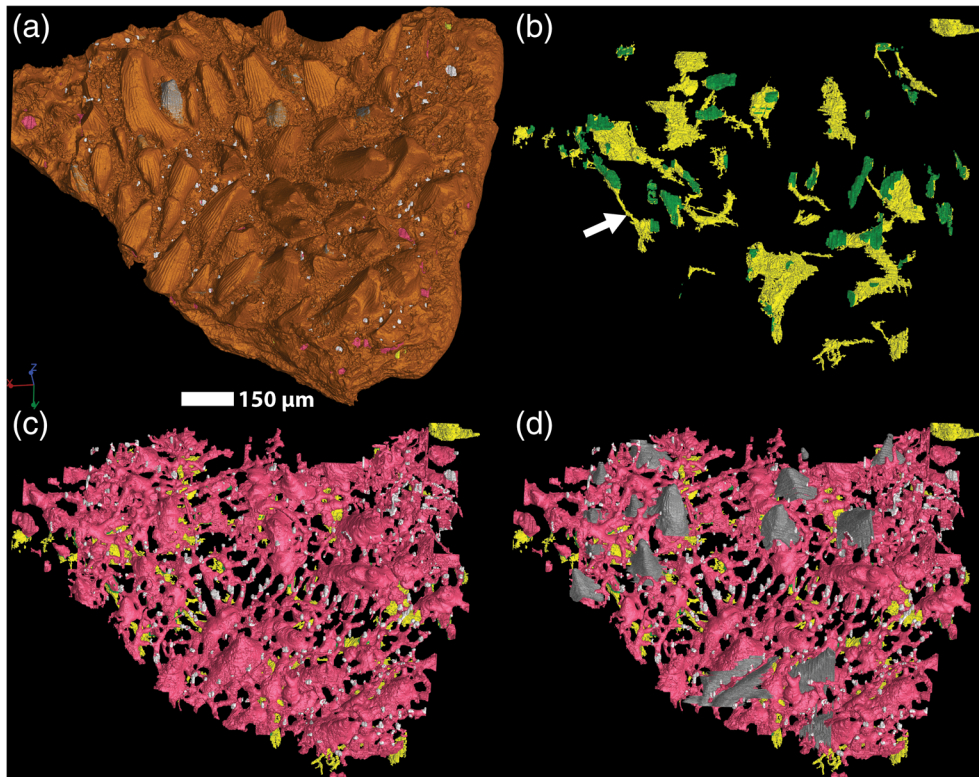


FIGURE 2 Three-dimensional models of the *Procephalaspis oeselensis* head shield fragment (GIT 769-17). Hard tissues (brown), basal cavities and canals (yellow), and lower mesh canals (pink). Contacts between basal canals and lower mesh canals are indicated with green, and openings of mesh canals to the surface are colored white. Buried tubercles have been colored gray in (a) and (d). Arrow in (b) points to a narrow canal connecting basal cavities. The element is oriented with its anterior pointing toward lower left

surfaces form tubercles (Figure 2(a),(d)) that are either partly or completely covered by younger generations of tubercles. Therefore, some of the smaller tubercles visible at the surface are actually the exposed tips of older generations (Figure 2(a)).

The cavities of the basal layer in the *P. oeselensis* head shield fragment are relatively small and scattered throughout the basal layer (Figure 2(b)), and narrower canals connect the cavities occasionally (arrow in Figure 2(b)). Similar to all of the other investigated taxa, they only open to the canals of the middle layer in a few places.

The middle layer has a deep set of mesh canals just above the basal layer, which also includes the cavities of the oldest and often buried tubercles (Figures 1(a) and 2(c)). The deepest canals acquire a radial appearance where they connect three separate areas composing the head shield fragment (Figure 2(c)). The separate cavities of each tubercle in *P. oeselensis* also have canals that radiate away from them (Figure 2(c)), which was also pointed out by Denison (1951). The cavities of the younger generations of tubercles in *P. oeselensis* and their associated horizontal canal network lie above the deep canal network, but connect to it extensively. It is noteworthy that there are no pore fields present where the mesh canals open to the surface, or at the former openings that surround buried tubercles in *P. oeselensis* (Figure 1(a)).

3.2 | *Aestiaspis viitaensis*

The head shield of *A. viitaensis* (Figure 3(a)) shows evidence of superpositional growth, as the tubercles sometimes overlie older generations, essentially fusing with them on the surface and effectively forming a single large tubercle (arrowhead in Figure 1(b)).

The basal cavities of *A. viitaensis* are irregular and only occupy a narrow band of the head shield fragment anteriorly (Figure 3(b)). The basal layer itself thins out toward the posterior part of this fragment, where it forms a smooth rim, but the tissue and canals of the middle layer extend beyond this border.

The *A. viitaensis* head shield fragment has larger, curved mesh canals that run in an antero-posterior direction with perpendicular connections between them, as well as a couple of thicker perpendicular canals in the posterior part of the head shield fragment (Figure 3(c)). There is no clear relation between larger mesh canals and the tubercles on the surface. Instead, the larger mesh canals form an irregular network. Thin and winding offshoots from the large mesh canals supply the subepidermal vascular plexus of the tubercles, while other vertical canals open to the surface. The canals in *A. viitaensis* open to the surface through pore fields (Afanassieva & Märss, 1997), but these are only sometimes preserved in the material investigated here (arrow in Figure 1(b)). Most of the openings are overarched by modified tubercles with a T-like cross-section (left in Figure 1(b)), that effectively produce partially enclosed upper canals. These partially enclosed canals form paired streaks between tubercles (teal in Figure 3(d)) that appear to be relatively independent from the mesh canal system of the middle layer, as are the tubercles at large, and connect to the mesh canal system in different places.

3.3 | *Dartmuthia gemmifera*

The head shield fragment of *D. gemmifera* investigated here (Figure 4) probably comes from a more posterior and lateral part of the head

FIGURE 3 Three-dimensional models of the *Aestiaspis viitaensis* head shield fragment (GIT 769-29). The colors indicate the same as in previous figures with the addition of partially/semi-enclosed upper canals (teal) and highlighted pore fields/perforated septa (white). Arrow in (b) points to a narrow canal connecting basal cavities. The element is oriented with its anterior pointing toward lower left

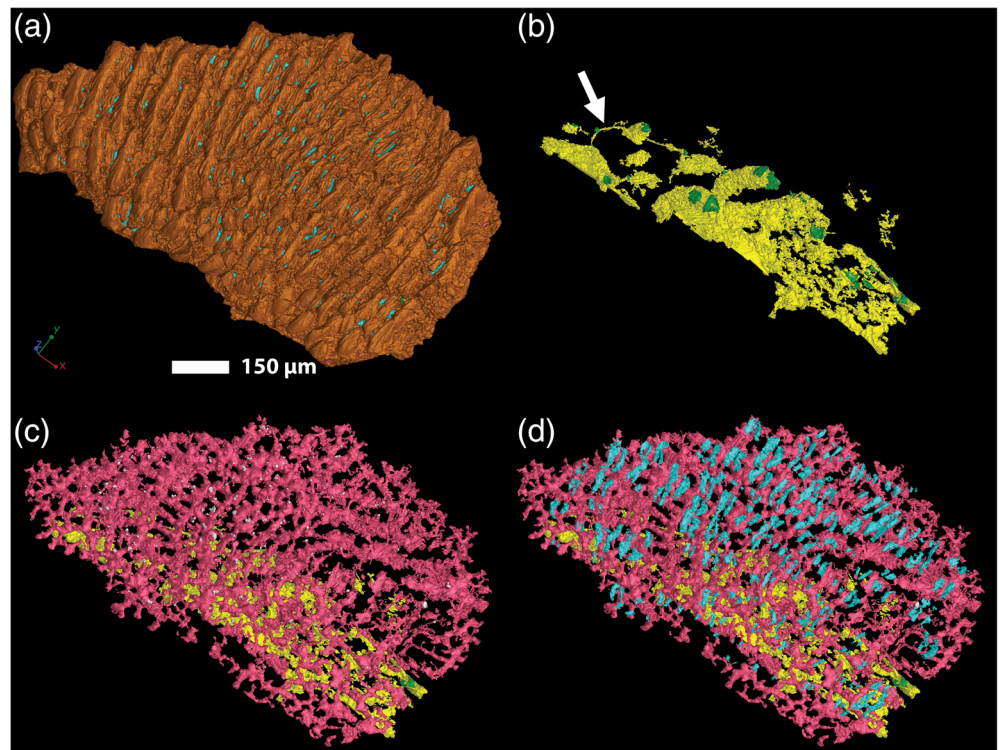
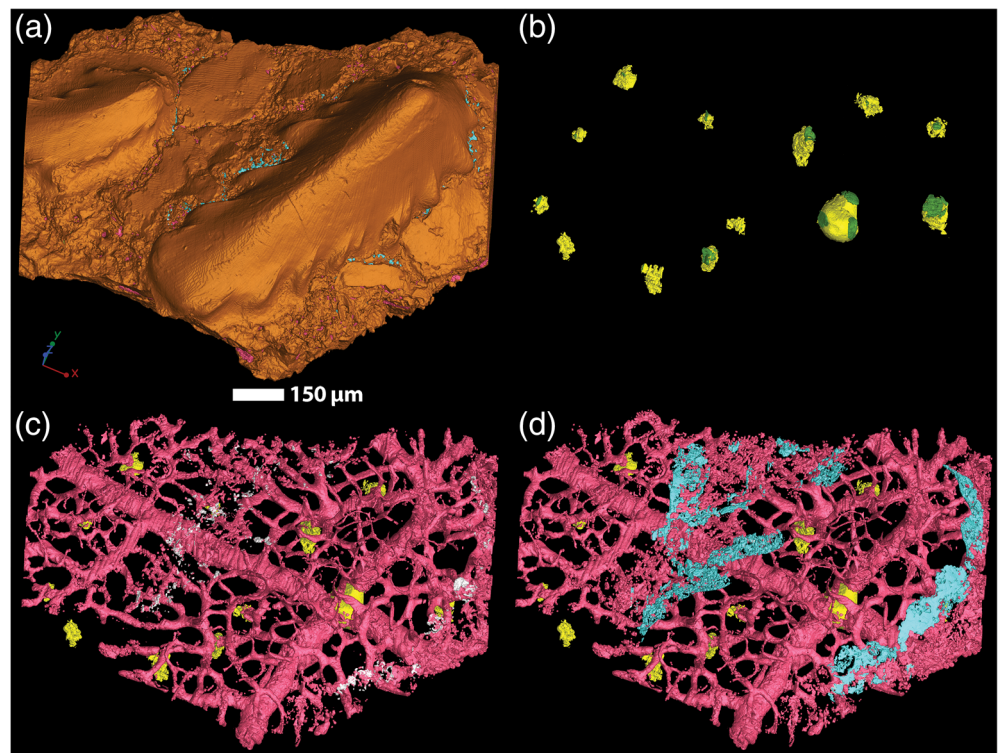


FIGURE 4 Three-dimensional models of the *Dartmuthia gemmifera* head shield fragment (GIT 769-25). Colors indicate the same as in previous figures. The element is oriented with its anterior pointing toward lower left



shield judging by the outstretched and slightly curved tubercle (compare to Märss et al., 2014, fig. 11I). No natural borders are preserved and part of it was cropped in the scanning procedure (Figure 4(a)). Unfortunately, the areas creating the semi-enclosed upper canals are poorly preserved in this fragment (Figure S1A), so a scale of

D. gemmifera (Figure 5) is also included in this study in order to investigate this part more closely. The basal layer of scales generally differed from the head shield in the thyestiid *T. mammillata* (O'Shea et al., 2019). There were also some other topological differences between them, but the general histology of the middle and upper

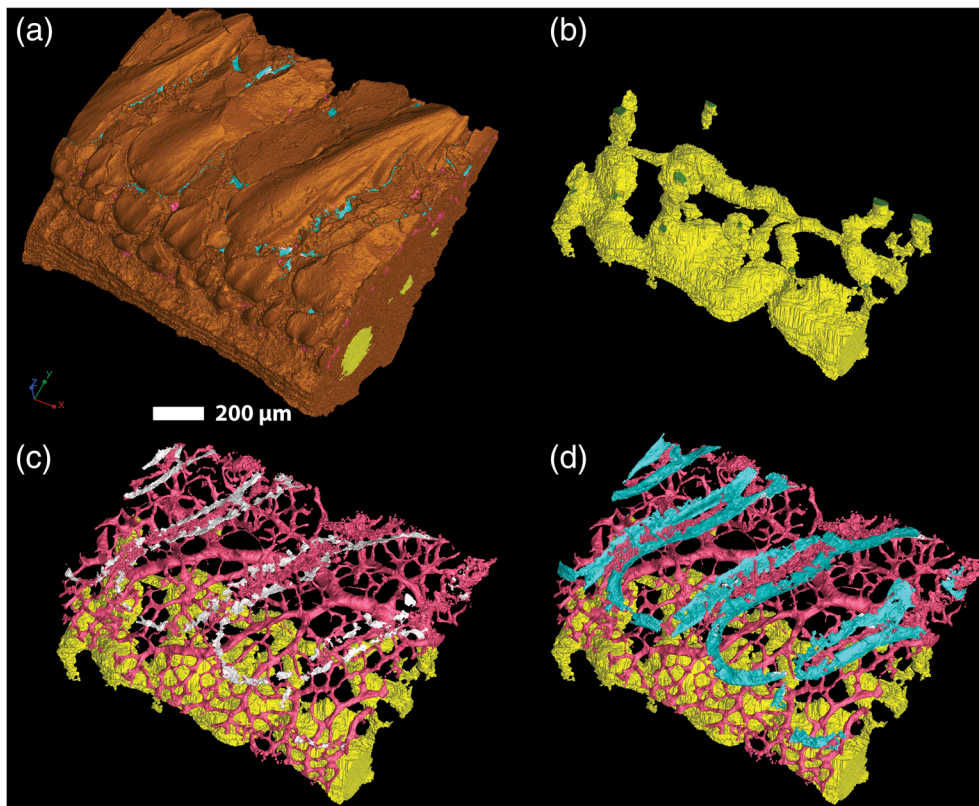


FIGURE 5 Three-dimensional models of the *Dartmuthia gemmifera* scale (GIT 769-24). Colors indicate the same as in previous figures. The element is oriented with its anterior pointing toward lower left

layer was similar as they produced similar structures, which is evident in the material studied here as well.

The basal layer of the *D. gemmifera* head shield fragment is relatively thin and consists of large fiber bundles (Figure S1A), and only a few scattered and pillar-like canals are present (Figure 4(b)). The largest, vertical canal running through the basal layer and opening to the basal surface has, unlike all other taxa, conspicuously smooth walls (Figure S1A and Figure 4(b)). It also has a thin, inner lining of unclear nature, which is most likely not a primary structure, but the walls of the basal layer itself are smooth as well. The scale of *D. gemmifera* has a few isolated, pillar-like canals in its basal layer, as well as some larger cavities, that are interconnected by relatively large and almost horizontal canals (Figures 1(c) and 5(b)).

The head shield fragment has two main and large mesh canals that run deeper than the remaining mesh canal system (Figure 4(c) and Figure S1A), one of which follows the antero-posterior direction of the element while the other runs perpendicularly to it (Figure 4(c) and Figure S2A). The main canals intersect underneath the largest tubercle, where they also connect to the conspicuously smooth basal canal described above (Figure 4(c) and Figure S1A), but there is no large cavity formed in the middle layer under the largest tubercles. There is another antero-posteriorly running mesh canal that connects to the main perpendicular canal (Figure 4(c)), but it is not as large and positioned vertically higher. The remainder of the mesh canal system is irregularly branching and sits higher up in the middle layer. However, slightly larger canals appear to converge at the center of each section created between the two main mesh canals, where they also connect to basal canals (Figure 4(b),(c) and Figure S2A). There are a

few connections between the mesh canal system and the basal canals in other parts of the head shield fragment as well. Numerous thinner canals rise from the mesh canal system to supply the subepidermal vascular plexus of both the larger tubercles, as well as the tessera-like tubercles in-between that reach over the perforated septa (Figure 4(d)). Other mesh canals ascend from the deeper mesh canal network and reach toward the contact with the upper canal system (Figure 4(c)). The areas underneath the tessera-like tubercles are poorly preserved in the head shield fragment (Figure S1A), so it is difficult to see the extent of the perforated septa and the canals underlying it. The deepest mesh canals do not have a radial layout, but some of the ascending mesh canals appear radial as they reach away from the large tubercles (on the right in Figure 4(d)).

The largest mesh canal of the *D. gemmifera* scale is deep and irregularly branching (Figure 5(c)). Besides this, the mesh canal system of the middle layer branch seemingly independently from the surface structures, and even the largest tubercles lack a large cavity or any trace of one (Figure 5(a),(c)). However, mesh canals ascend into both the large tubercles and the tessera-like plates that cover the bony septum. Other ascending mesh canals reach toward the perforated septum and expand horizontally to underlie the entirety of it, sometimes forming continuous meandering canals underneath (Figure 5(c)). Because these meandering canals often are connected to the canal system underlying the large tubercles, the canals that run away from the tubercles obtain a radiating appearance in the scale as well (bottom right in Figure 5(c)). The circular canals that were described in *D. gemmifera* by Afanassieva (2004) have not been identified in the head shield fragment or the scale.

The perforated septum in *D. gemmifera* is more extensive compared to the smaller clusters of pores in *A. viitaensis*. As stated before, the semi-enclosed upper canals of the *D. gemmifera* head shield fragment are poorly preserved (Figure 4(d)), but are much better preserved in the scale where they form an extensive network between larger tubercles (Figure 5(d)). The modified tubercles in *D. gemmifera* are more extensively abutting to each other compared to the modified tubercles in *A. viitaensis*, and the semi-enclosed upper canal system that they create is only open to the surface through grooves between them.

3.4 | *Tremataspis* species

The *Tremataspis* material investigated here resembles that described for *T. mammillata* by O'Shea et al. (2019). The head shield fragments of both *T. mammillata* (Figure 6 and Figure S1B) and *T. milleri* (Figures 1(d) and 7) have rounded basal cavities throughout the basal layer with some connections between them. In general, each polygon of upper mesh canals has a basal cavity underneath them, but there are some exceptions (e.g., center of Figure 6(b)). Furthermore, one of these bulbous cavities lacks connections to the mesh canals of the middle layer (center-right in Figure 7(b)). The head shield of *T. schmidtii*

lacks a basal layer entirely (Figure S1C), which is possibly related to its growth stage, as demonstrated in *T. mammillata* by Denison (1947, fig. 11). *Tremataspis perforata* (Figure 9 and Figure S1D) is only represented by scales in this study, which explains some of the observed histological (mainly in the basal layer) and topological differences. This taxon was described solely based on disarticulated material by Märss et al. (2014) because it had a much more discontinuous surface and larger, irregular pores compared to other *Tremataspis* species, and it is included here in order to study these peculiarities. In accordance to what was observed in scales of *T. mammillata* (O'Shea et al., 2019), the basal cavities and canals in the *T. perforata* scale do not show the same regular layout. Instead, most of the basal layer is occupied by one large and irregular cavity (Figure 9(b)).

Following the discovery of a perforated septum separating the mesh canals in three species of *Tremataspis* (Bölauf, 1951; Denison, 1947), subsequent works have divided this canal system into lower and upper parts (e.g., Qu et al., 2015), with the septum itself being composed of bone (O'Shea et al., 2019). Because the upper mesh canal system is viewed as separate from the lower mesh canal system, it will be described separately below. The lower mesh canal system of *Tremataspis* has a polygon-like organization where it underlies the bony septum below the upper mesh canal system. This is best seen in *T. mammillata*, where lower mesh canals underlie the entirety

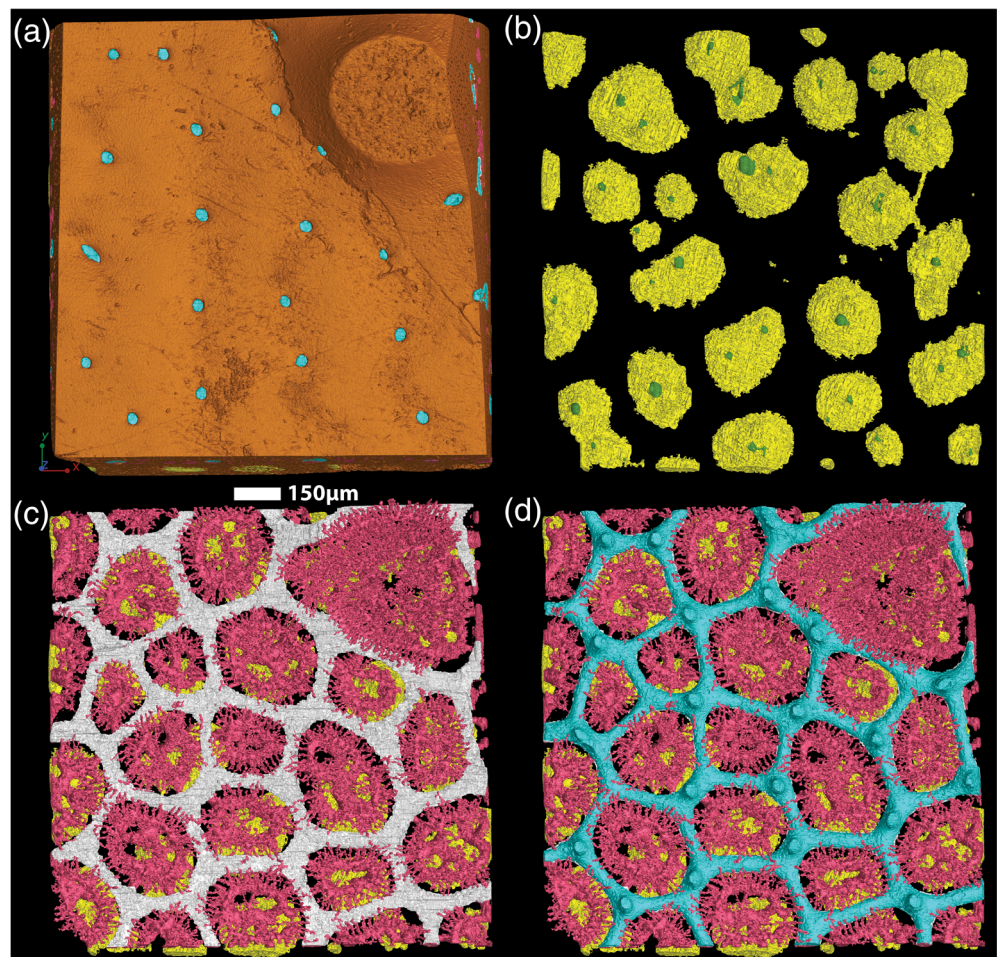


FIGURE 6 Three-dimensional models of the *Tremataspis mammillata* head shield fragment (GIT 769-20). Colors indicate the same as in previous figures, but teal represents the upper mesh canal system

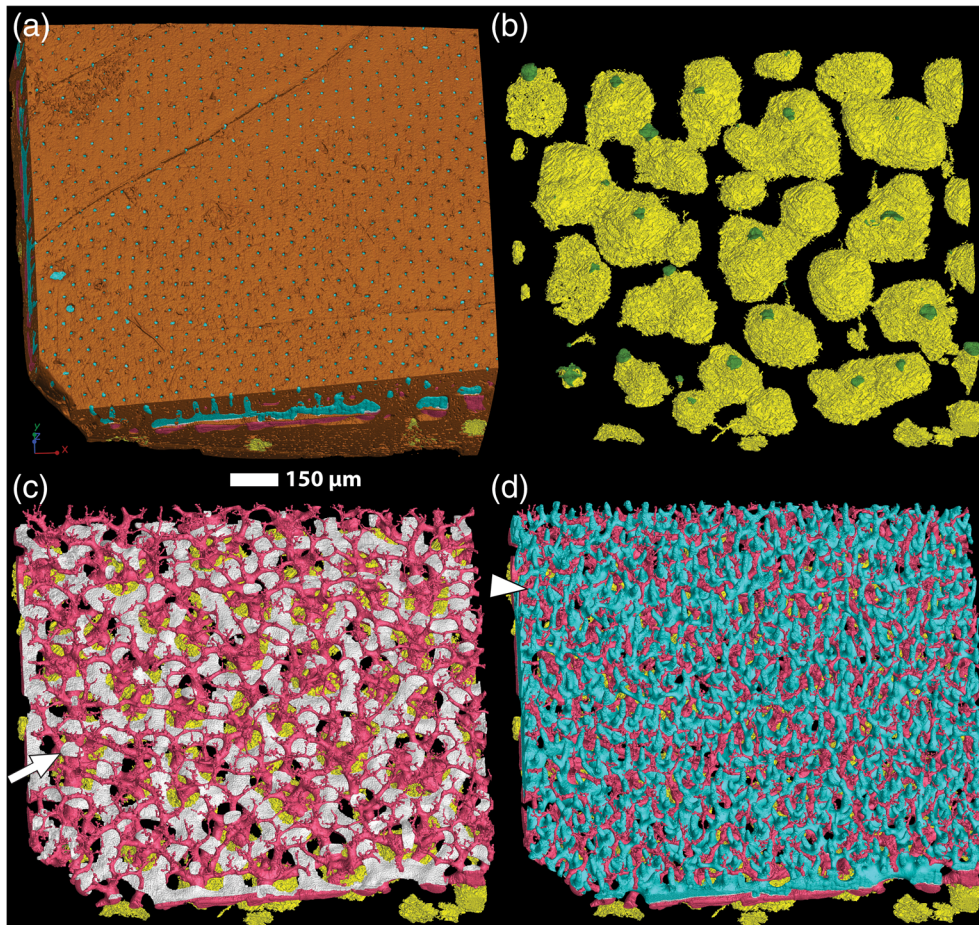


FIGURE 7 Three-dimensional models of the *Tremataspis milleri* head shield fragment (GIT 769-1). Colors indicate the same as in previous figures. The arrow in (c) points to a perforated septum within a polygon and the arrowhead in (d) points to a forked ascending canal of the upper mesh canal system

of the upper mesh canal system (Figure 6(c)). Within the polygons of *T. mammillata*, the lower mesh canals form loops that connect to the surrounding lower mesh canals (Figure 6(c) and Figure S2B). In some places, these connections continue between adjacent loops and form an irregularly branching network (Figure S2B). The loops also send narrower canals toward the surface that form the subepidermal vascular plexus that supply the dentine of the continuous superficial layer (center of Figure S1B). The narrow canals that arise from the lower mesh canal system reach above the upper mesh canals toward the tips of similar canals from neighboring polygons, but they do not appear to connect (Figure 6(c)). Furthermore, each loop has a connection to the basal cavities, although they may sometimes be small, or only open into minuscule and blind basal canals (center of Figure 6(b)). The polygonal architecture of the lower mesh canal system is interrupted under the large tubercle-like surface structure (top right in Figure 6(c)). Instead, three loop-like sections with separate connections to basal cavities appear to have merged under this surface structure (lower right in Figure S2B).

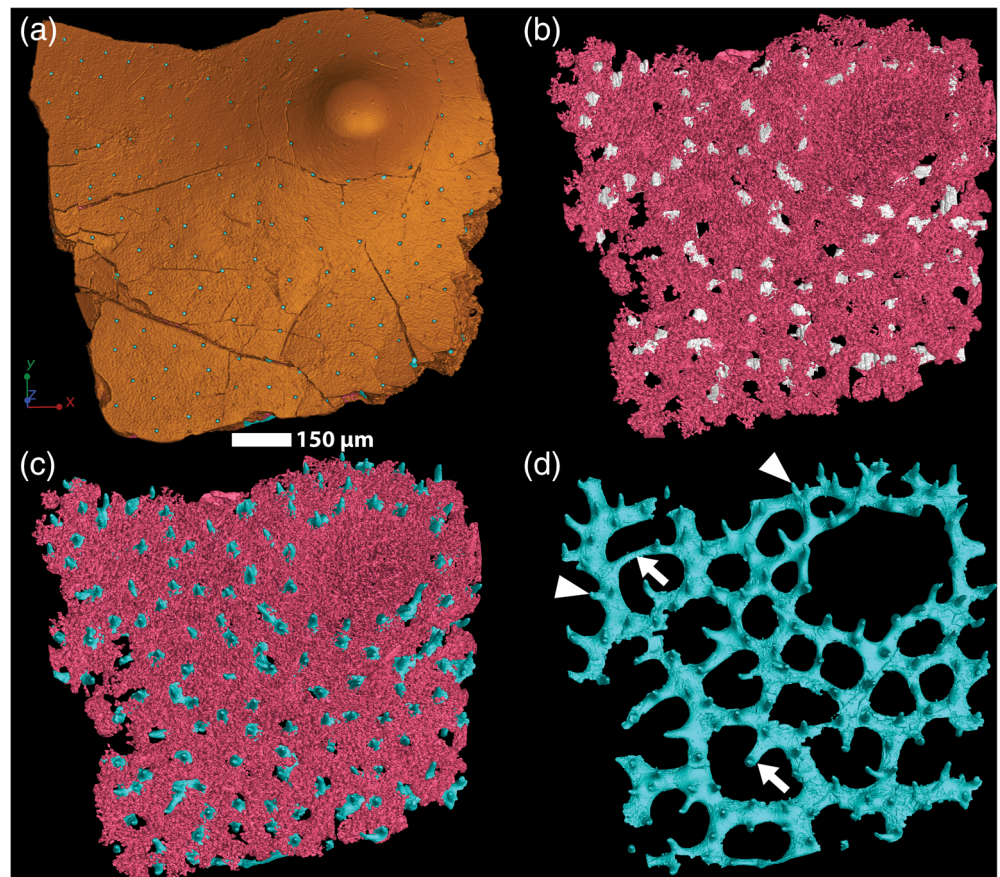
The majority of the lower mesh canal system in *T. milleri* also forms a polygonal network that reflects the architecture of the upper mesh canal system with a bony septum between them (Figure 7(c)), but there are also independent and tree-like lower mesh canals (Figure S2C) similar to *T. mammillata*. Unlike *T. mammillata*, however, there are additional, intra-polygonal upper mesh canals within the

larger polygons in *T. milleri* (Figure 7(c)) at a higher level compared to the largest upper mesh canals (Figure 1(d)). Only a few of these intra-polygonal upper mesh canals have an equivalent in the lower mesh canal system and a bony septum separating them (arrowhead in Figure 7(c)), but most of them do not (see below). Another big difference compared to *T. mammillata* is that the canals of the lower mesh canal system within the polygons, which rise to supply the subepidermal vascular plexus, actually connect to mesh canals of adjacent polygons above the upper mesh canals (Figures 1(d) and 7(c),(d)). This was also reported by Denison (1947) in both *T. milleri* and *T. schmidtii*.

As mentioned before, the *T. schmidtii* head shield fragment studied here (Figure 8) has not been fully ossified because it is in a younger growth stage (compare Figure S1C to Denison, 1947, fig. 11B). Therefore, much of the lower mesh canal architecture remains obscure (Figure 8(b)). However, the majority of it must have attained a polygonal pattern because it underlies most of the upper mesh canal system (Figure S3), as it does in *T. mammillata*, and which was evident in the scale of *T. schmidtii* investigated by Qu et al. (2015, fig. 2F).

The *T. perforata* scale has, similar to the *D. gemmifera* scale, a deeper and independently branching system of lower mesh canals (Figure 9(c) and Figures S1D and S2D), although they are more numerous. Above this, the lower mesh canals underlying the perforated septum form an independent and more polygonally arranged canal system (Figure 9(d)) similar to that found in the head shields of the

FIGURE 8 Three-dimensional models of the *Tremataspis schmidtii* head shield fragment (GIT 769-11). Colors indicate the same as in previous figures. Arrowheads in (d) point to paired or forked ascending canals of the upper mesh canal system. Arrows in (d) point to a complete (top) and incomplete (bottom) intra-areal canal



other *Tremataspis* taxa. The polygonal and the deeper lower mesh canal systems are connected in some places through vertical canals, while other lower mesh canals ascend from the deeper lower mesh canal system and reach up into the polygons to supply the subepidermal vascular plexus (Figure 9(e)). In some places there are also horizontal canals connecting these mesh canals to the polygonally arranged lower mesh canals surrounding them.

In *Tremataspis* species, the upper mesh canal system is entirely enclosed within hard tissues, except for more or less regularly spaced pores that open to the surface. Subsequently, the entire surface in many *Tremataspis* taxa is covered by a continuous mesodentine layer with a hypermineralized cap, which is only pierced by these pores (Figures 6(a), 7(a), and 8(a)). In *T. mammillata*, the polygonal upper mesh canal network consists of large polygons with a continuous perforated septum connecting it to the lower mesh canal system (Figure 6(d)). The relatively large pores on the surface connect to vertical canals of the upper mesh canal system that arise at the intersections of the polygonal canals, or halfway in-between intersections (Figure 10(a)).

The upper mesh canal system in the head shield of *T. milleri* (Figure 7(d)) has large, main canals that are continuously connected to the lower mesh canal system through a perforated septum (Figure 7(c)). However, as mentioned before, *T. milleri* has additional upper mesh canals within the larger polygons, (Figure 10(b)), here termed intra-polygonal upper mesh canals. These further subdivide the polygons into

smaller areas and lie vertically higher than the largest upper mesh canals (Figure 1(d)). As described before, some of these intra-polygonal canals host at least a partial perforated septum with an equivalent canal of the lower mesh canal system (arrowhead in Figure 7(c)). Additional upper mesh canals that are much thinner and positioned even higher compared to all the other upper mesh canals further subdivide the polygons (Figures 7(d) and 10(b)), but these do not have any perforated septa or equivalent lower mesh canals. There are many more canals rising to the surface from the upper mesh canal system in *T. milleri* compared to *T. mammillata*, and subsequently the pores are more tightly spaced on the surface (Figure 7(a)). Furthermore, the majority of the ascending canals split into two toward the surface and give rise to two pore openings (e.g., arrowhead in Figure 7(d)).

The upper mesh canal system of *T. schmidtii* (Figure 8(c),(d)) is architecturally intermediate between *T. mammillata* and *T. milleri*. It mainly consists of wider, main canals with a continuous perforated septum connecting it to an equivalent canal of the lower mesh canal system (Figure S3). However, the polygons are not as clear as they are in *T. mammillata* and *T. milleri*, and there are only a few intra-polygonal canals (Figure 10(c)). The intra-polygonal canals are sometimes complete (top arrow in Figure 8(d)), but often only consist of an offshoot from the main upper mesh canals that approach the center of a polygon where it opens as a pore on the scale surface (bottom arrow in Figure 8(d)). The pore openings on the surface are denser in *T. schmidtii* when compared to *T. mammillata*, but

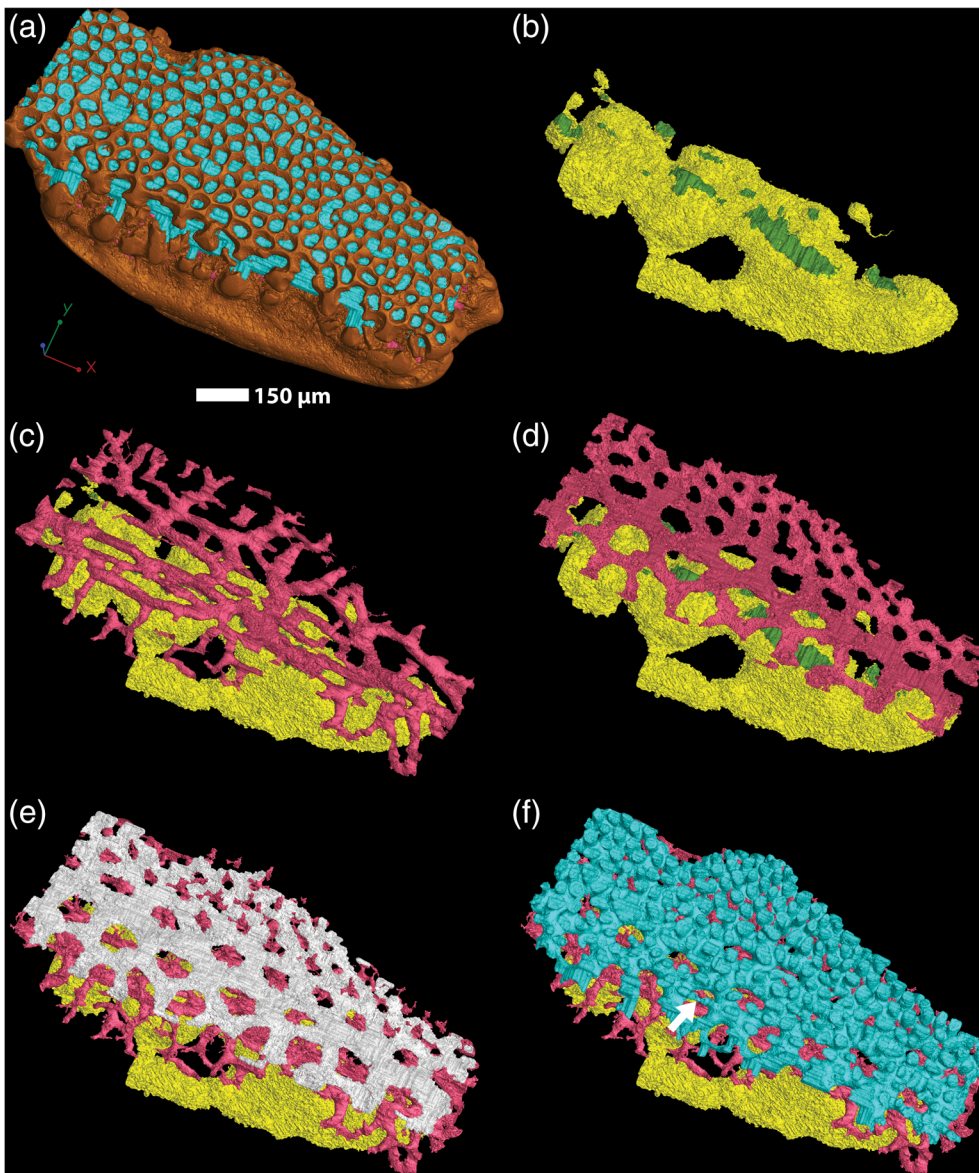


FIGURE 9 Three-dimensional models of the *Tremataspis perforata* scale (GIT 769-15). Colors indicate the same as in previous figures. (c) only contains the deepest set of lower mesh canals and (d) only contains the slightly higher positioned and polygonally arranged lower mesh canals. (e) contains all lower mesh canals with the perforated septum indicated in white. Arrow in (f) points to a smaller and vertically higher positioned upper mesh canal

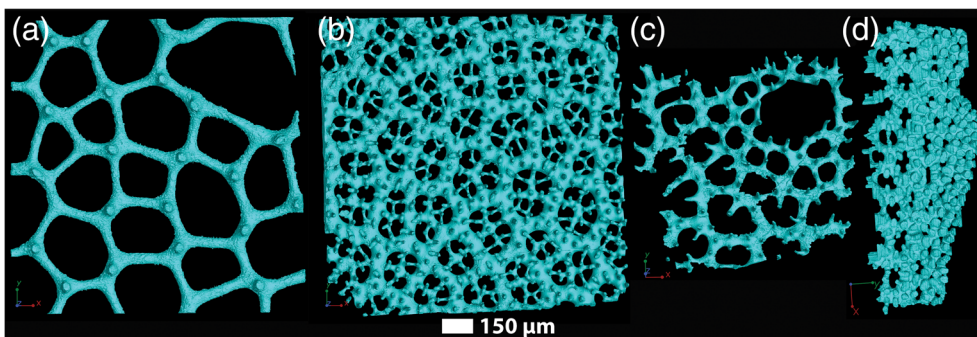
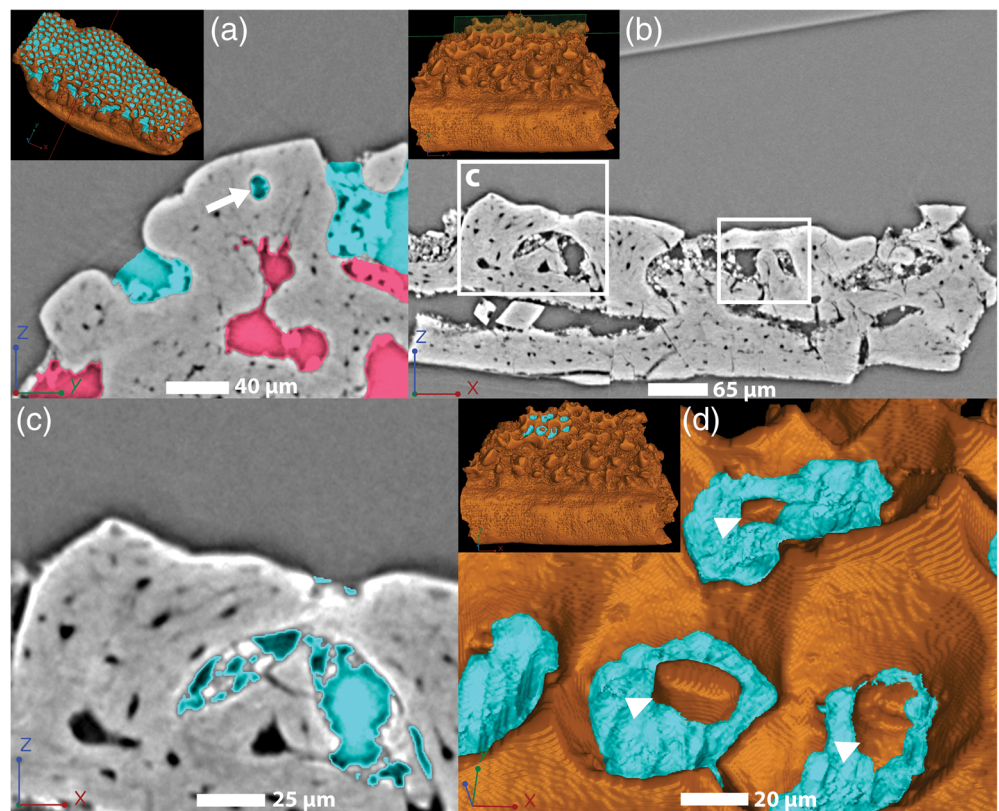


FIGURE 10 Three-dimensional models of the upper mesh canal system from each *Tremataspis* taxon investigated in this study in a top-down view and at the same scale. (a) *T. mammillata*; (b) *T. milleri*; (c) *T. schmidtii*; (d) *T. perforata*. The scale element in (d) is oriented with its anterior facing left

not as dense as in *T. milleri*. Furthermore, the majority of the ascending canals leading to pores are singular as in *T. mammillata*, but they can sometimes be paired, or fork into two toward the surface (arrowheads in Figure 8(d)), as in *T. milleri*.

The surface of the *T. perforata* scale (GIT 769-15) is not as smooth and continuous as the elements from other *Tremataspis* taxa (Figure 9(a)) and as a result, the enclosed upper mesh canals have several irregular and large openings to the surface (Figure 9(f)). The upper

FIGURE 11 (a) Detailed virtual scan slice of the small upper mesh canal enclosed within a modified, tubercle-like structure (arrow) in the *Tremataspis perforata* scale (GIT 769-15); (b) virtual scan slice of the other *T. perforata* scale (GIT 769-16) with rectangles indicating overgrown tubercle-like structures; (c) detail of the tubercle overarched by hard tissues with upper mesh canals highlighted in (b); (d) detail of scale surface and pore openings of the second *T. perforata* scale with arrowheads indicating the tips of overgrown tubercles within the pore openings. Colors indicate the same as in previous figures



mesh canals leading to the surface openings branch off seemingly randomly from the entirely enclosed and polygonally arranged upper mesh canal network situated below (Figure 9(f)), and they are much more irregularly placed compared to the other *Tremataspis* taxa (Figure 10(a),(d)). The largest polygons are of similar dimensions as in *T. schmidti* (Figure 10(d)), but further comparisons between scales and head shields may prove fruitless (O'Shea et al., 2019). There are also a few fully enclosed, intra-areal upper mesh canals in this taxon as well (arrow in Figure 9(f)). This intra-areal canal appears to have formed within a single modified tubercle (arrow in Figure 11(a)). The second scale of *T. perforata* (GIT 769-16) investigated here is much more chaotic in its inner structure (Figure 11(b)) and has not been fully modeled out for this reason. However, in this specimen some of the upper canals clearly formed between separate, individual tubercle-like structures that sometimes fuse or overgrow each other (Figure 11(b),(c)). In fact, the tips of buried tubercles are sometimes visible inside the surface pores of the upper mesh canals (arrowheads in Figure 11(d)).

4 | DISCUSSION

4.1 | Comparisons to previous histological studies

Buried tubercles in *P. oeselensis* were shown in a histological sketch by Janvier (1996, fig. 4.17A), but the original publication identifies the investigated specimen as a *Cephalaspis* sp. from Spitsbergen (Ørvig, 1951, fig. 11B). We agree that the specimen is similar to

P. oeselensis, but its identity remains unclear. However, overgrowth of tubercles in *P. oeselensis* was later pointed out by Märss et al. (2014, fig. 33V) and it is evident by the material investigated here that the dermal elements of this taxon formed partially by superpositional growth of tubercles that were supplied by a shallower vascular network higher up in the middle layer. The dermal elements of *A. viitaensis* also formed, at least in part, by overgrowth of new tubercles on top of older ones, but the remaining taxa in this study do not show any buried surfaces. However, *T. perforata* have tubercles covered by later generations of hard tissues, and rare cases of overgrowth observed in *T. milleri* (Märss et al., 2014, fig. 7K, L) suggests that the capability of appositional growth was retained in other thyeistiids (O'Shea et al., 2019). Denison (1952) used size data to conclude that *T. mammillata*, unlike some other osteostracans (Hawthorn et al., 2008; Keating et al., 2012), probably had a determinate growth and that its hard tissues only formed when its shield was fully grown. Denison (1947) showed different stages of development in *T. mammillata*, where the youngest specimen only showed ossification of a continuous, thin outer dentine and enameloid cover, and the only ossification of the middle layer was found directly surrounding the polygonally arranged lower and upper mesh canals (Denison, 1947, fig. 11A). At later growth stages, the middle layer would become increasingly ossified (Denison, 1947, fig. 11B, C) and the last layer to form was the basal layer that thickened toward the base (Denison, 1947, fig. 11C, D). A single mineralization phase of an encapsulating head shield further supports a determinate growth in *T. mammillata* and *Tremataspis* in general. Denison (1951) suspected

that *D. gemmifera* had a similar growth because one of his sectioned specimens lacked a basal layer and only had partially enclosed canals in the middle layer.

The *D. gemmifera* head shield fragment investigated here is unlike any head shield material previously investigated by both Wängsjö (1946: pl. 5, fig. 1) and Denison (1951, fig. 32C), where each tesserae with a large tubercle on the surface hosted a large central basal cavity. However, these features may depend on the life-position of the head shield fragments. The head shield fragment investigated here also has two main and large mesh canals that run deeper than the remaining mesh canal system, which is similar to what is observed in the scale of this taxon.

The presence of pore fields has been used as a synapomorphy for thyeistiid osteostracans, (e.g., Afanassieva & Märss, 1997; Sansom, 2008), but it should be mentioned that the *P. oeselensis* material used for this character by Sansom (2008) was first described as *Thyestes* sp. in Gross (1968b, fig. 12B, D, 13A–E). Fredholm (1990) later referred these to *Procephalaspis oeselensis*?, but this was challenged by Jarochowska et al. (2016) who again assigned them to *Thyestes* (although erroneously referring to Gross' fig. 11 instead of fig. 12). No signs of pore fields have been identified in the material studied here, but fragmentary material referred to this taxon shows a few openings with pore-like structures (Märss et al., 2014, fig. 34I). Furthermore, the canal openings often have a second layer forming a rim around the opening, which could indicate the former presence of a pore field (e.g., Märss et al., 2014, fig. 34I).

According to Afanassieva and Märss (1997), the pore fields in *A. viitaensis* may fuse in places to form a small, perforated septum, but this was not identified in the material studied here. Material from the dorsal side of the head shield of *D. gemmifera* presented by Wängsjö (1946) and Denison (1951) has extensive perforated septa overarched by modified tubercles that attain tessera-like morphologies. These sit in-between larger tubercles and create a semi-enclosed canal network (see also Gross, 1961). The same pattern was identified in both the head shield and scale fragments of *D. gemmifera* investigated in this study. The ventral side of the head shield in *D. gemmifera* on the other hand, lacks the large tubercles and is instead entirely covered by modified and tessera-like tubercles, which effectively forms a continuous, polygonal network of semi-enclosed upper canals (see Denison, 1951). Previous studies have pointed out the similarity of both the perforated septum and the polygonal network of these semi-enclosed canals in *D. gemmifera* to the upper mesh canal system found in *Tremataspis*.

The upper mesh canals of the *T. mammillata* head shield investigated here are similar to those in the head shield described by O'Shea et al. (2019). Lower mesh canals underlie the entirety of the upper mesh canal system in both the head shield (Figure 6(c)) and scales (O'Shea et al., 2019) of *T. mammillata*. The lower mesh canals reach above the upper mesh canals toward the tips of similar canals from neighboring polygons, but they do not appear to connect in *T. mammillata* (Figure 6(c)) or *T. perforata* (Figure 9(f)). This was also reported for *T. mammillata* by Denison (1947) and in the material investigated by O'Shea et al. (2019). Both *T. schmidtii* and *T. milleri*,

however, have canals arising from the lower mesh canals within adjacent polygons that connect above the upper mesh canal system (Figure 7(d); Qu et al., 2015, fig. 2C). Furthermore, *T. milleri* has intrapolygonal upper mesh canals, that were homologized by both Stensiö (1932) and Denison (1951) to the intra-areal canals described in cephalaspids (see below).

4.2 | Potential homologies of canal systems

The deeper mesh canals that acquire a radial appearance in the *P. oeselensis* head shield fragment are reminiscent to the radial canals described in cephalaspids by Stensiö (1927, 1932). Radial canals in cephalaspids constituted the deepest set of vascular canals that ran parallel to the external surface of the dermal elements and radiated out from the center of each tessera to connect to the radial canals of neighboring tesserae (Stensiö, 1927, 1932). According to Afanassieva (1999), radiating canals are also present in the early-branching osteostracan *Ateleaspis*, which suggests that it is plesiomorphic for osteostracans (O'Shea et al., 2019). Wängsjö (1952) drew comparisons between the deepest, but often irregular, vascular canals in several thyeistiid taxa to the radial canals of other osteostracans, and Afanassieva and Märss (2014) homologized the network of deeper mesh canals in *A. viitaensis* to the radial canals of other osteostracans. The radially arranged canals surrounding large tubercles in *D. gemmifera* have also been homologized to the deep radial canals of other osteostracans (Afanassieva, 1995; Wängsjö, 1946). However, Gross (1961) stated that this could not be the case because they occur much higher in the middle layer compared to the deeply underlying radial canals proper, which is supported by the data presented here.

The potential homology between the semi-enclosed upper canal system of *D. gemmifera* to the pore-canal system of *Tremataspis* has been suggested before (e.g., Afanassieva, 1995; Denison, 1951). The similarity is perhaps best seen between the ventral shield of *D. gemmifera* (Denison, 1951, fig. 33A) and *T. mammillata* (Figure 6(d)). Considering the phylogenetic framework presented by Sansom (2008, 2009), a version of this system can be seen in *A. viitaensis* (Figure 3(d)), where modified tubercles partially overhang pore fields. Further modification of the morphology of these tubercles into tessera-like plates could form the more continuous, semi-enclosed upper canal system seen in *D. gemmifera* (Figure 5(d)). The dorsal head shield of *D. gemmifera* often has a large tubercle at the center of what appears to be proper tesserae, which in turn is surrounded by smaller and tessera-like, modified tubercles (Wängsjö, 1946: pl. 5 fig. 1). These tessera-like tubercles overhang a perforated septum and essentially form a semi-enclosed upper canals system. According to Wängsjö (1946), however, they are all of similar dimensions, so there was no way of distinguishing between upper canals occurring between and within the tesserae proper. The vasculature of the tessera-like tubercles is positioned higher up in the middle layer and they essentially overgrow the flanks of the larger tubercles, which is also the case in the scale studied here (Figure 1(c): tessera-like

tubercle). On the ventral side of the head shield, however, it appears that each main tubercle of the tesseræ proper has been modified to overhang the perforated septa that border them (Denison, 1951, fig. 32B). The superficial similarity between the semi-enclosed upper canal system of the ventral head shield in *D. gemmifera* to the polygonal network of upper mesh canals seen in *T. mammillata* has led to suggestions that the large polygonal canals in the latter represent borders between tesseræ (Stensiö, 1927).

Stensiö (1927, 1932) described so-called mucus canals in cephalaspids that were divided into inter-areal canals (at the borders between tesseræ) and intra-areal canals (between tubercles within tesseræ). In cephalaspids that had a continuous superficial layer, both the inter- and intra-areal canals were entirely enclosed in hard tissues and only opened to the surface through pores, but they did not arise from and were not connected to the subepidermal vascular plexus (Stensiö, 1932 contra Stensiö, 1927). Therefore, the inter- and intra-areal canals were fully enclosed in more superficial tissues and formed a canal system separate from the vasculature of the middle layer, which is similar to what is seen in *Tremataspis* (Stensiö, 1932). Following the comparison between *D. gemmifera* and *T. mammillata*, previous workers further homologized the different parts of the upper mesh canals in *Tremataspis* to the inter- and intra-areal canals of cephalaspids. However, unlike *Tremataspis*, the canals in cephalaspids only connected to the mesh canals of the middle layer in a few places (Stensiö, 1932, fig. 6) and not through a continuous perforated septum.

Qu et al. (2015) interpreted the upper mesh canals in *T. schmidtii* as epithelial invaginations, having smooth walls as a result of mesodentine initiating its growth at an epithelium-mesenchyme interface within the canals and growing away from it. This was also observed in *T. mammillata* by O'Shea et al. (2019). O'Shea et al. (2019) further suggested that the upper mesh canals represent partial boundaries between regions of odontogenesis, because the vasculature (the lower mesh canals) of each polygon had no clear connections to each other above the upper mesh canals (e.g., Figure 6(d)). However, as pointed out by Denison (1947), and which is visible in the material presented here, the lower mesh canals of each polygon connect extensively to each other above the upper mesh canals in both *T. milleri* and *T. schmidtii*, essentially fusing the vasculature of each region (Figure 7(d)). The largest upper mesh canals in these two taxa are of similar dimensions as the upper mesh canals in *T. mammillata* (Figure 10(a),(b)), but there are also additional upper mesh canals within the polygons (i.e., intra-polygonal canals) that are positioned at a higher vertical level, some of which has a short perforated septum underlying it. Some of these intra-polygonal upper mesh canals also has lower mesh canals reaching over and connecting above them (Figure 7(d)). Furthermore, some of the smaller upper mesh canals in *T. perforata* appears to have formed within a modified tubercle itself (Figures 9(f) and 11(a)).

Because there are generally no preserved traces of odontode-generations or centers of tesseræ in *Tremataspis*, and because the shape of an odontode dictates the underlying vasculature (see Donoghue, 2002), it is not possible to determine if the upper mesh

canals in *Tremataspis* represent borders between tesseræ or tubercles. Furthermore, some of the smaller canals in *T. perforata* seem to have formed within modified tubercles themselves. A distinction between inter- and intra-areal canals seems difficult to make in *D. gemmifera* as well (Wängsjö, 1946). For these reasons, it is not possible to establish a homology between the polygonal and intra-polygonal upper mesh canals in *Tremataspis* to the inter- and intra-areal canals of cephalaspids, as suggested by Stensiö (1927, 1932). However, the results of this study strongly support the homology between the upper mesh canal system in *Tremataspis* to the partially and semi-enclosed upper canals of other thyeistiids.

4.3 | The emergence of a pore-canal system in *Tremataspis*

O'Shea et al. (2019) explained the regular architecture of the polygonal network in *T. mammillata* with the odontode regulation theory presented by Reif (1982). Essentially, the mutual inhibition of dermal papillae would regulate the growth of odontodes in a reaction-diffusion system (see Cooper et al., 2018; Donoghue, 2002; Maisey & Denton, 2016). This also reconciled the single phase of mineralization with the "growth lines" that had been identified in some *Tremataspis* specimens (Denison, 1947; Janvier, 1985), by identifying them as the breakdown of Turing patterning (O'Shea et al., 2019). Indeed, the occurrence of tessera-like plates that sometimes attained more tubercle-like morphologies on the dorsal head shield of *D. gemmifera* (Gross, 1961; Wängsjö, 1946) point to similar areas of inhibition operating in this taxon as well. The reaction-diffusion mechanism fits well with the pattern of the polygonal system in both *D. gemmifera* and *T. mammillata*, where each tessera or polygon could represent a region of odontogenesis that are separate from each other because the lower mesh canals do not connect between them (O'Shea et al., 2019). However, this model is complicated by other *Tremataspis* species that have additional upper mesh canals within the polygons, as well as connections between the lower mesh canals of neighboring polygons above the upper mesh canals. The upper mesh canals in *T. milleri* can be divided into four levels (Figure 12(a),(b)): the inter-polygonal upper mesh canals (Number 1 in Figure 12), the largest intra-polygonal upper mesh canals (Number 2 in Figure 12) that subdivide the polygon into 2–4 areas, and two levels of smaller intra-polygonal upper mesh canals (Numbers 3 and 4 in Figure 12) that further subdivide the polygon. As stated before, the lower mesh canal system connects regularly above the largest upper mesh canals (Number 1 in Figure 12(c)), and often over the intra-polygonal upper mesh canals as well (Number 2 in Figure 12(c)). The intra-polygonal upper mesh canals also appear to be influenced by the deeper generations of upper mesh canals that they connect with (Figure 12(b)). In theory, the same reaction-diffusion system could function in these *Tremataspis* taxa as well, if the area of inhibition changed over time and subsequently enabled the formation of new tubercles within polygons. The deeper tubercles observed in *T. perforata* that were in turn covered by hard tissues to form additional upper mesh canals certainly indicate such a

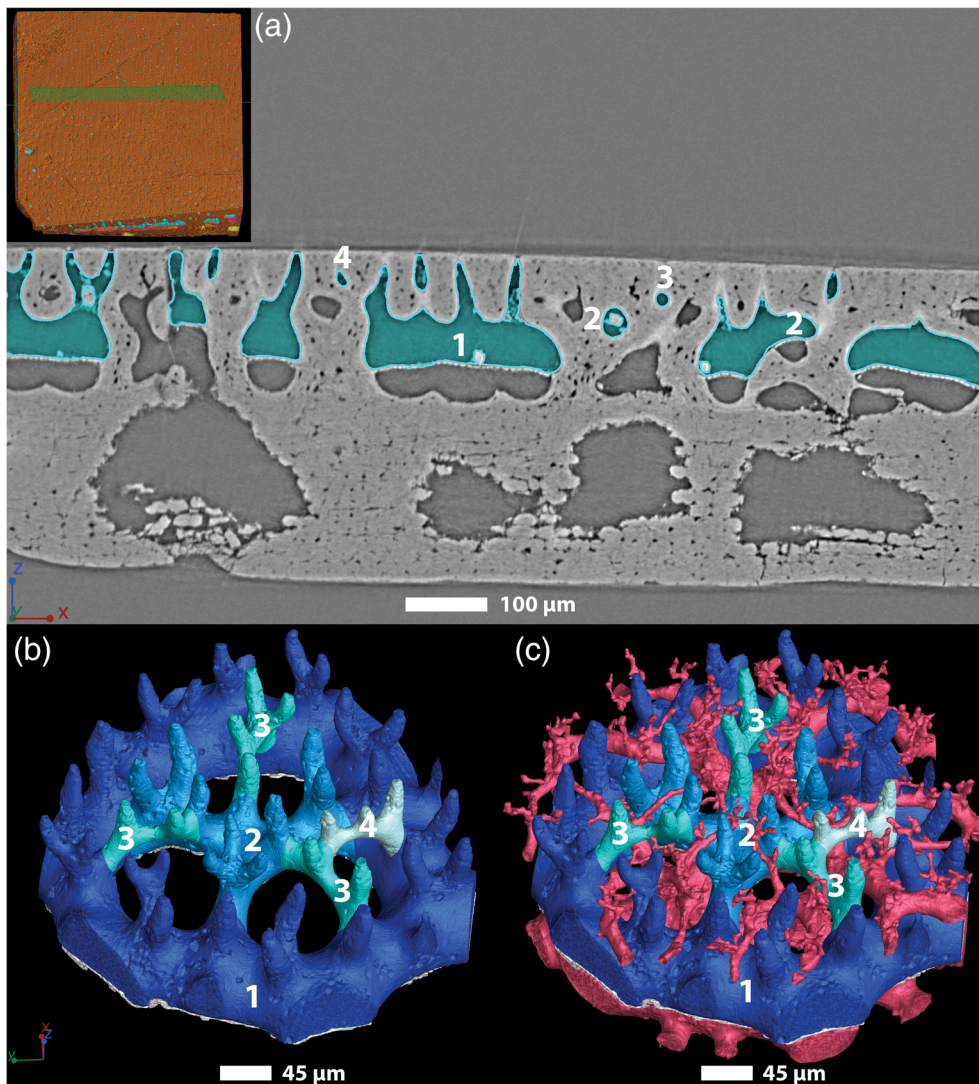


FIGURE 12 (a) Virtual scan slice of the *Tremataspis milleri* head shield fragment (GIT 769-1) with numbers 1–4 indicating different levels of upper mesh canals (teal); (b)–(c) three-dimensional models of a single polygon from the same dermal element with the lower mesh canals (pink) and four levels of upper mesh canals in different shades of blue (labeled with numbers 1–4); (c) the relation between the upper mesh canals to the lower mesh canal system and the subepidermal vascular plexus. Note that the basal cavities and canals have not been included or highlighted

development. Alternatively, the upper canals could have formed by modifications of the tubercles themselves, and both modes of formation appear to have occurred in the *T. perforata* scales. However, the complete lack of any traces of this preserved in hard tissues makes it difficult to discern the actual development of the dermal elements in most of the investigated *Tremataspis* material.

Considering the growth stages presented by Denison (1947) for *Tremataspis*, and the lack of primary odontodes or extensive remodeling in the canal system of *T. mammillata* (O'Shea et al., 2019), its dermal skeleton was most likely embedded in a single phase of mineralization. The scans of *T. milleri* and *T. schmidtii* also lack buried tubercles or any signs of major remodeling (Figure 1(d)), indicating a single phase of mineralization in these taxa as well. As pointed out by O'Shea et al. (2019), the growth of *Tahulaspis* (*Zenaspis*? sp. indet. sensu Gross, 1961) suggests the presence of an upper mesh canal system in the dermis between a first generation of odontodes, which is eventually covered by a second generation of hard tissue formation. The initial formation of a continuous surface of enameloid and dentine

that encapsulated both the surface of the dermal element and the upper mesh canal system below (Denison, 1947; O'Shea et al., 2019) points to the prior existence of a similar network in soft tissues in *Tremataspis* as well. Qu et al. (2015) suggested that the upper mesh canals in *T. schmidtii* formed by invaginations of the epithelium. The different levels of upper mesh canals in *T. milleri* could therefore have formed by subsequent invaginations of epithelium in conjunction with a thickening of the dermis. In such a system, the outer surface together with the upper mesh canals would represent a continuous mesenchyme-epithelium contact. However, no direct trace of this is preserved in the hard tissues.

The phylogenetic framework presented by Sansom (2008, 2009) makes it possible to present a tentative model for the emergence of the upper mesh canal system in *Tremataspis* (Figure 13). The overgrowth of tubercles observed in *P. oeselensis* (Figure 13(a)) can be seen to a certain degree in *A. viitaensis* as well (Figure 13(b)). *Aestiaspis viitaensis* also has modified tubercles overarching pore fields, and tubercles are further modified into tessera-like plates in *D. gemmifera*

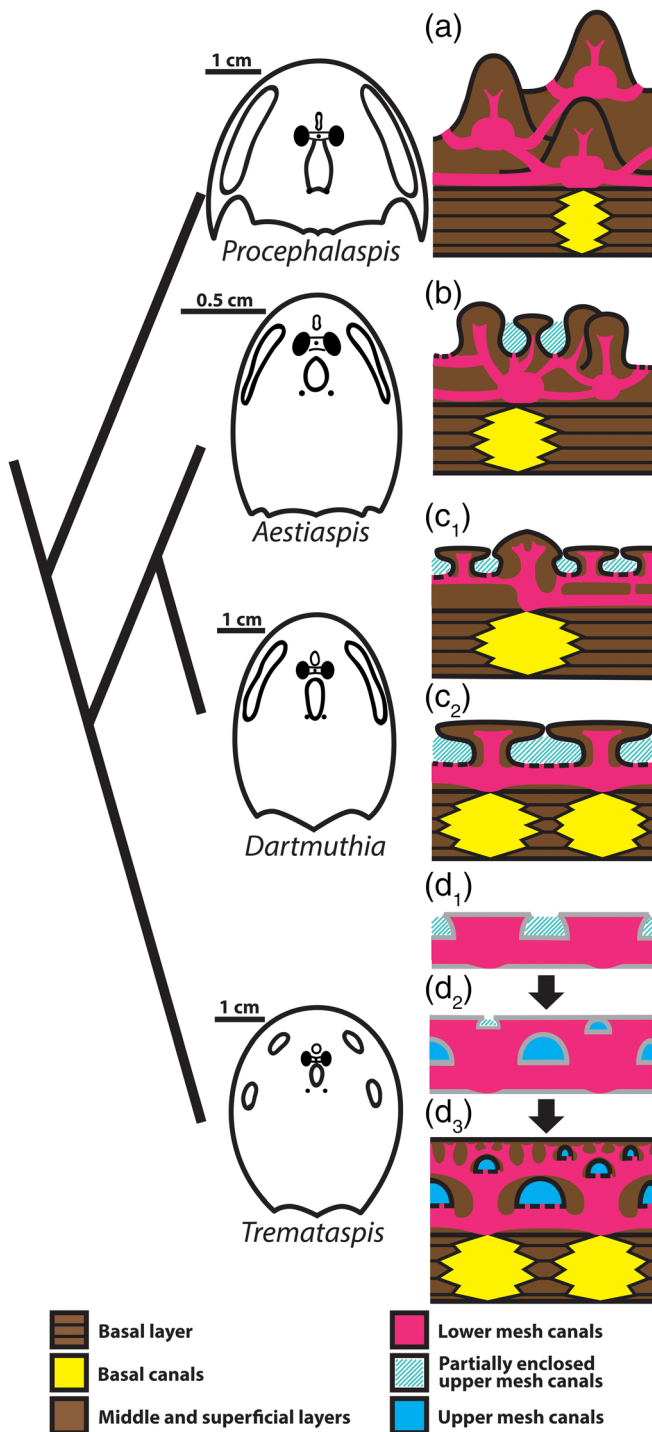


FIGURE 13 Phylogenetic relations and head shield outlines of the thyeistiid taxa included in this study. The schematics to the right illustrate the suggested growth of hard tissues in each taxon. (a) *Procephalaspis oeselensis*; (b) *Aestiaspis viitaensis*; (c) *Dartmuthia gemmifera* with dorsal (C1) and ventral (C2) head shield structure inferred from Denison (1951, fig. 32B, C); (d) *Tremataspis milleri* with the possible development (indicated by black arrows) of soft tissues ((d1) and (d2)) and hard tissues after a single mineralization stage (d3). The lower mesh canals are expanded in (d1) and (d2) to represent presumed soft tissues

(Figure 13(c)). The dorsal head shield in *D. gemmifera* has a younger network of vasculature supplying the secondary, modified tubercles developing around each main tubercle (Figure 13(c1)), while the ventral head shield (Figure 13(c2)) could represent the previously mentioned reaction-diffusion system with a single generation of tubercles. The overgrowth of hard tissues in *P. oeselensis* and *A. viitaensis* potentially gave way to a single mineralization phase in most *Tremataspis*. The upper mesh canals in *T. perforata* appear to have formed both between tubercles and within modified tubercles themselves, but it is not possible to deduce how the upper mesh canals formed in other *Tremataspis* because no trace of this is preserved in their hard tissues. In another thyeistiid, namely *Thyestes verrucosus*, a growth model was presented by Afanassieva (2014) where the earliest mineralized parts of tesserae had no contact with the mineralized parts of neighboring tesserae during growth, which suggests a delayed onset of mineralization. In such a scenario, much of the framework in *Tremataspis* could have formed in soft tissues first, with subsequent invaginations of epithelium (Figure 13(d1),(d2)) before the initiation of mineralization in the adult-sized animal (Figure 13(d3)), as postulated by Denison (1947).

5 | CONCLUSIONS

The tessellate condition of the dermal skeleton is generally considered plesiomorphic for osteostracans (Janvier, 1996). In many groups, the deepest vasculature is composed of radial canals that emanate from the center of each tessera and eventually connect to the radial canals of neighboring tesserae (Afanassieva, 1999; Stensiö, 1927, 1932; Wängsjö, 1952). Furthermore, the central part of each tessera generally has a group of basal cavities and canals underlying it (Stensiö, 1927; Wängsjö, 1952). The pattern of both the basal and deepest mesh canals seen in the *P. oeselensis* head shield fragment presented here (Figure 2(b),(c)) could reflect the condition seen outside of Thyeistiida. This pattern appears to be lost in other thyeistiids, where the deepest mesh canals form a much more irregular network (see also O'Shea et al., 2019; Qu et al., 2015; Wängsjö, 1952), but the basal canals become increasingly more regular in their layout. The regularly placed, large basal cavities seen in both *D. gemmifera* and *Tremataspis* have often been viewed as indicating separate tesserae (Denison, 1947; Wängsjö, 1946), although their relation to the vasculature of the middle layer may differ in detail (Wängsjö, 1946). For example, the descending canals at tessera-borders described in cephalaspids appear to be missing in *D. gemmifera* (Wängsjö, 1946). Because the dermal elements of *T. mammillata* is superficially similar to the ventral head shield of *D. gemmifera*, its upper mesh canal system was considered homologous to the semi-enclosed upper canal system of *D. gemmifera*. Because of this, and because each polygon is generally underlain by a basal cavity, Denison (1951) also viewed them as homologous to the inter-areal canals of other osteostracans. A polygonal network of canals is often present in osteostracans, although they may range from open grooves to fully enclosed canals

(Stensiö, 1932; Wängsjö, 1952). This study confirms the primary homology between the semi-enclosed upper canals in *D. gemmifera* to the upper mesh canals in *Tremataspis* as a whole. However, because there are no traces of tubercle generations preserved in the hard tissues of most *Tremataspis*, it is less clear whether the inter-polygonal canals reflect borders between tesseræ or tubercles. For the same reason, it is not possible to say whether the upper mesh canals in *Tremataspis* could equate to the inter- and intra-areal canals of other osteostracans. However, it is possible that both *Tremataspis* and other osteostracans embedded a canal system that existed ancestrally in soft tissues, as suggested by Stensiö (1932), although they differ in detail (e.g., the perforated septum dividing the canal system is only present in thyeistiids).

It is clear that the complex pore-canal system in *Tremataspis* evolved through the modification of the semi-enclosed canal system present in closely related thyeistiids. In turn, the semi-enclosed system in *D. gemmifera* was produced by modifying the growth and shape of superficial tubercles. However, it is not possible to homologize the different parts of the upper mesh canal system between different thyeistiids, or to similar canal systems of other osteostracans. Similar investigations on a wider array of taxa may produce phylogenetically informative traits that can help test potential homologies and help us acquire a better understanding of the dermal hard tissues in osteostracans in general. In extension, this may help elucidate the origin and evolution of the dermal skeleton in jawed vertebrates.

ACKNOWLEDGMENTS

The authors would like to thank the reviewers for their input, which greatly improved this work. We also thank Ursula Toom, Tallinn, for help connected with the loan of material. The experiments were performed on beamline ID19 at the European Synchrotron Radiation Facility (ESRF, proposal ES 581) in Grenoble, France. We acknowledge the European Synchrotron Radiation Facility for provision of synchrotron radiation facilities and for assistance in using beamline ID19. T.M. acknowledges the Department of Geology at TTU for allowing her to use their facilities for research.

CONFLICT OF INTEREST

The authors have no conflict of interest.

AUTHOR CONTRIBUTIONS

Oskar Bremer: Investigation, data modeling, visualization, writing original draft. **Qingming Qu:** Conceptualization, writing review and editing. **Sophie Sanchez:** Conceptualization, data acquisition, writing review and editing. **Tiiu Märss:** Specimen acquisition, writing review and editing. **Vincent Fernandez:** Scan session setup, writing original method section and review text. **Henning Blom:** Conceptualization, data acquisition, project administration, writing review and editing.

PEER REVIEW

The peer review history for this article is available at <https://publons.com/publon/10.1002/jmor.21359>.

DATA AVAILABILITY STATEMENT

The data that support the findings of this study are openly available in the ESRF database (<http://paleo.esrf.eu/>).

ORCID

Oskar Bremer  <https://orcid.org/0000-0002-3310-9374>

Vincent Fernandez  <https://orcid.org/0000-0002-8315-1458>

REFERENCES

- Afanassieva, O. B. (1995). The structure of the exoskeleton of the Tremataspidoidei and its significance in the taxonomy of osteostracans (Agnatha). *Geobios*, 28, 13–18.
- Afanassieva, O. B. (1999). The exoskeleton of *Ungulaspis* and *Ateleaspis* (Osteostraci, Agnatha) from the lower Devonian of Severnaya Zemlya, Russia. *Acta Geologica Polonica*, 49(2), 119–123.
- Afanassieva, O. B. (2004). Subclass Osteostraci. Osteostracans. In N. L. I. & A. O. B. (Ed.), *Fossil vertebrates of Russia and adjacent countries. Agnathans and early fishes* (pp. 210–267). 436 pp. [In Russian with English summary on pp 420–421]. GEOS.
- Afanassieva, O. B. (2014). Development of the exoskeleton in Osteostracans (Agnatha, vertebrata): New evidence of growth. *Paleontological Journal*, 48(9), 973–979.
- Afanassieva, O. B., & Märss, T. (1997). Exoskeleton structure and the distribution of *Aestiaspis viitaensis* (Agnatha) from the Silurian of Estonia. *Paleontological Journal*, 31(6), 641–647.
- Afanassieva, O. B., & Märss, T. (2014). New data on the exoskeleton of the osteostracan genus *Aestiaspis* (Agnatha) from the Silurian of Saaremaa Island (Estonia) and the Severnaya Zemlya archipelago (Russia). *Paleontological Journal*, 48(1), 74–78.
- Berg, L. S. (1940). Classification of fishes, both recent and fossil. *Trudy Zoologicheskogo Instituta, Akademiya Nauk SSSR*, 5, 346–517.
- Börlau, E. (1951). Das Sinnesliniensystem der Tremataspiden und dessen Beziehungen zu anderen Gefässsystemen des Exoskeletts. *Acta Zoologica*, 32(1-2), 31–40.
- Cooper, R. L., Thiery, A. P., Fletcher, A. G., Delbarre, D. J., Rasch, L. J., & Fraser, G. J. (2018). An ancient Turing-like patterning mechanism regulates skin denticle development in sharks. *Science Advances*, 4(11), 1–10.
- Denison, R. H. (1947). The exoskeleton of *Tremataspis*. *American Journal of Science*, 245(6), 337–365.
- Denison, R. H. (1951). The exoskeleton of early Osteostraci. *Fieldiana: Geology*, 11(4), 199–218.
- Denison, R. H. (1952). Early Devonian fishes from Utah: Part 1. Osteostraci. *Fieldiana Geology*, 11(6), 265–287.
- Denison, R. H. (1966). The origin of the lateral-line sensory system. *American Zoologist*, 6(3), 368–370.
- Donoghue, P. C. J. (2002). Evolution of development of the vertebrate dermal and oral skeletons: Unraveling concepts, regulatory theories, and homologies. *Paleobiology*, 28(4), 474–507.
- Donoghue, P. C. J., Sansom, I. J., & Downs, J. P. (2006). Early evolution of vertebrate skeletal tissues and cellular interactions, and the canalization of skeletal development. *Journal of Experimental Zoology Part B: Molecular and Developmental Evolution*, 306(3), 278–294. <https://doi.org/10.1002/jez.b.21090>
- Fredholm, D. (1990). Agnathan vertebrates in the lower Silurian of Gotland, Sweden. *GFF*, 112(1), 61–80.
- Gross, W. (1935). Histologische studien am aussenskelett fossiler Agnathen und Fische. *Palaeontographica Abteilung A*, 83, 1–60.
- Gross, W. (1956). Über Crossopterygier und Dipnoer aus dem baltischen Oberdevon im Zusammenhang einer vergleichenden Untersuchung des Porenkanalsystems paläozoischer Agnathen und Fische. *Kungliga Svenska Vetenskapsakademiens Handlingar*, 5(6), 140.

- Gross, W. (1961). Aufbau des Panzers obersilurischer Heterostraci und Osteostraci Norddeutschlands (Geschiebe) und Oesels. *Acta Zoologica*, 42(1-2), 73–150.
- Gross, W. (1968a). Beobachtungen mit dem Elektronenraster-Auflichtmikroskop an den Siebplatten und dem Isopedin von Dartmuthia (Osteostraci). *Paläontologische Zeitschrift*, 42(1-2), 73–82.
- Gross, W. (1968b). Die Agnathen-fauna der silurischen Halla-Schichten Gotlands. *GFF*, 90(3), 369–400.
- Hawthorn, J. R., Wilson, M. V., & Falkenberg, A. B. (2008). Development of the dermoskeleton in *Superciliaspis gabrielsei* (Agnatha: Osteostraci). *Journal of Vertebrate Paleontology*, 28(4), 951–960.
- Janvier, P. (1985). Les Thyestidiens (Osteostraci) du Silurien de Saaremaa (Estonie). Première Partie: Morphologie et Anatomie. *Annales de Paléontologie (Vertebres-Invertébrés)*, 71(2), 83–147.
- Janvier, P. (1996). *Early vertebrates*. Oxford University Press.
- Jarochowska, E., Bremer, O., Heidlas, D., Pröpster, S., Vandenbroucke, T. R. A., & Munnecke, A. (2016). End-Wenlock terminal Mulde carbon isotope excursion in Gotland, Sweden: Integration of stratigraphy and taphonomy for correlations across restricted facies and specialized faunas. *Palaeogeography, Palaeoclimatology, Palaeoecology*, 457, 304–322. <https://doi.org/10.1016/j.palaeo.2016.06.031>
- Keating, J. N., Sansom, R. S., & Purnell, M. A. (2012). A new osteostracan fauna from the Devonian of the Welsh borderlands and observations on the taxonomy and growth of Osteostraci. *Journal of Vertebrate Paleontology*, 32(5), 1002–1017. <https://doi.org/10.1080/02724634.2012.693555>
- King, B., Hu, Y., & Long, J. A. (2018). Electroreception in early vertebrates: Survey, evidence and new information. *Palaeontology*, 61(3), 325–358.
- Lyckegaard, A., Johnson, G., & Tafforeau, P. (2011). Correction of ring artifacts in X-ray tomographic images. *International Journal of Tomography and Statistics*, 18, 1–9.
- Maisey, J. G., & Denton, J. S. (2016). Dermal denticle patterning in the cretaceous hybodont shark *Tribodus limae* (Euselachii, Hybodontiformes), and its implications for the evolution of patterning in the chondrichthyan dermal skeleton. *Journal of Vertebrate Paleontology*, 36(5), e1179200.
- Märss, T., Afanassieva, O., & Blom, H. (2014). Biodiversity of the Silurian osteostracans of the East Baltic. *Earth and Environmental Science Transactions of the Royal Society of Edinburgh*, 105(02), 73–148. <https://doi.org/10.1017/s1755691014000218>
- Mirone, A., Brun, E., Gouillart, E., Tafforeau, P., & Kieffer, J. (2014). The PyHST2 hybrid distributed code for high speed tomographic reconstruction with iterative reconstruction and a priori knowledge capabilities. *Nuclear Instruments and Methods in Physics Research Section B: Beam Interactions with Materials and Atoms*, 324, 41–48.
- Mondéjar-Fernández, J. (2018). On cosmine: Its origins, biology and implications for sarcopterygian interrelationships. *Cybium*, 42(1), 41–65.
- Ørving, T. (1951). Histologic studies of Placoderms and fossil elasmobranchs. I: The endoskeleton, with remarks on the hard tissues of lower vertebrates in general. *Arkiv för Zoologi*, 2(2), 321–454.
- Ørving, T. (1967). Phylogeny of tooth tissues: Evolution of some calcified tissues in early vertebrates. In A. E. W. Miles (Ed.), *Structural and chemical organization of teeth* (pp. 45–110). Academic Press.
- O'Shea, J., Keating, J. N., & Donoghue, P. C. (2019). The dermal skeleton of the jawless vertebrate *Tremataspis mammillata* (Osteostraci, stem-Gnathostomata). *Journal of Morphology*, 280(7), 999–1025.
- Paganin, D., Mayo, S. C., Gureyev, T. E., Miller, P. R., & Wilkins, S. W. (2002). Simultaneous phase and amplitude extraction from a single defocused image of a homogeneous object. *Journal of Microscopy*, 206(1), 33–40.
- Qu, Q., Blom, H., Sanchez, S., & Ahlberg, P. (2015). Three-dimensional virtual histology of Silurian osteostracan scales revealed by synchrotron radiation microtomography. *Journal of Morphology*, 276(8), 873–888. <https://doi.org/10.1002/jmor.20386>
- Qu, Q., Sanchez, S., Zhu, M., Blom, H., & Ahlberg, P. E. (2017). The origin of novel features by changes in developmental mechanisms: Ontogeny and three-dimensional microanatomy of polyodontode scales of two early osteichthyans. *Biological Reviews of Cambridge Philosophical Society*, 92(2), 1189–1212. <https://doi.org/10.1111/brv.12277>
- Reif, W.-E. (1982). Evolution of dermal skeleton and dentition in vertebrates: The odontode regulation theory. *Evolutionary Biology*, 15, 287–368.
- Sansom, R. S. (2008). The origin and early evolution of the Osteostraci (vertebrata): A phylogeny for the Thyestiida. *Journal of Systematic Palaeontology*, 6(3), 317–332. <https://doi.org/10.1017/s1477201907002386>
- Sansom, R. S. (2009). Phylogeny, classification and character polarity of the Osteostraci (vertebrata). *Journal of Systematic Palaeontology*, 7(1), 95–115. <https://doi.org/10.1017/s1477201908002551>
- Schultze, H.-P. (2016). Scales, enamel, cosmine, ganoine, and early osteichthyans. *Comptes Rendus Palevol*, 15(1-2), 83–102.
- Sire, J. Y., Donoghue, P. C., & Vickaryous, M. K. (2009). Origin and evolution of the integumentary skeleton in non-tetrapod vertebrates. *Journal of Anatomy*, 214(4), 409–440.
- Smith, M. M., & Hall, B. K. (1993). A developmental model for evolution of the vertebrate exoskeleton and teeth. *Evolutionary Biology*, 27, 387–448.
- Stensiö, E. A. (1927). *The Downtonian and Devonian vertebrates of Spitsbergen. Part I, Family Cephalaspidae* (Vol. A. Text). Det Norske Videnskapsakademi i Oslo.
- Stensiö, E. A. (1932). *The Cephalaspids of Great Britain*. British Museum (Natural History).
- Thomson, K. S. (1977). On the individual history of cosmine and a possible electroreceptive function of the pore-canal system in fossil fishes. In S. M. Andrews, R. S. Miles, & A. D. Walker (Eds.), *Problems in vertebrate evolution* (pp. 247–271). Academic Press.
- Wang, N.-Z., Donoghue, P. C., Smith, M. M., & Sansom, I. J. (2005). Histology of the galeaspid dermoskeleton and endoskeleton, and the origin and early evolution of the vertebrate cranial endoskeleton. *Journal of Vertebrate Paleontology*, 25(4), 745–756.
- Wängsjö, G. (1946). On the genus *Dartmuthia* Patten, with special reference to the minute structure of the exoskeleton. *Uppsala University Bulletin of Geology*, 31, 349–362.
- Wängsjö, G. (1952). The Downtonian and Devonian vertebrates of Spitsbergen. IX. Morphologic and systematic studies of the Spitsbergen Cephalaspids. *Skifter Norsk Polarinstittutt*, 97, 1–657.

SUPPORTING INFORMATION

Additional supporting information may be found online in the Supporting Information section at the end of this article.

How to cite this article: Bremer O, Qu Q, Sanchez S, Märss T, Fernandez V, Blom H. The emergence of a complex pore-canal system in the dermal skeleton of *Tremataspis* (Osteostraci). *Journal of Morphology*. 2021;1–17. <https://doi.org/10.1002/jmor.21359>